Article

Neuron

Endolysosomal Deficits Augment Mitochondria Pathology in Spinal Motor Neurons of Asymptomatic fALS Mice

Highlights

- Lysosomal deficit is an early pathological event in fALS-linked hSOD1^{G93A} mouse MNs
- Reduced autophagic clearance contributes to mitochondrial pathology in fALS MNs
- hSOD1^{G93A} impairs retrograde transport by disturbing dynein-endosome coupling
- Enhancing endosome trafficking by snapin rescues autophagy-lysosomal deficits

Authors

Yuxiang Xie, Bing Zhou, Mei-Yao Lin, Shiwei Wang, Kevin D. Foust, Zu-Hang Sheng

Correspondence

shengz@ninds.nih.gov

In Brief

Xie et al. reveal progressive lysosomal deficits in motor neurons starting at asymptomatic stages in fALS-linked hSOD1^{G93A} mice, and the authors advance our understanding of early pathological mechanisms underlying motor neuron degeneration.

Xie et al., 2015, Neuron *87*, 355–370
July 15, 2015
http://dx.doi.org/10.1016/j.neuron.2015.06.026

Neuron
Article

Endolysosomal Deficits Augment Mitochondria Pathology in Spinal Motor Neurons of Asymptomatic fALS Mice

Yuxiang Xie,[1,3] Bing Zhou,[1,3] Mei-Yao Lin,[1] Shiwei Wang,[1] Kevin D. Foust,[2] and Zu-Hang Sheng[1,*]
[1]Synaptic Functions Section, The Porter Neuroscience Research Center, National Institute of Neurological Disorders and Stroke (NINDS), NIH, Room 2B-215, 35 Convent Drive, Bethesda, MD 20892-3706, USA
[2]Department of Neuroscience, Ohio State University, 698 BRT, 460 West 12th Avenue, Columbus, OH 43210, USA
[3]Co-first author
*Correspondence: shengz@ninds.nih.gov
http://dx.doi.org/10.1016/j.neuron.2015.06.026

SUMMARY

One pathological hallmark in ALS motor neurons (MNs) is axonal accumulation of damaged mitochondria. A fundamental question remains: does reduced degradation of those mitochondria by an impaired autophagy-lysosomal system contribute to mitochondrial pathology? We reveal MN-targeted progressive lysosomal deficits accompanied by impaired autophagic degradation beginning at asymptomatic stages in fALS-linked hSOD1^{G93A} mice. Lysosomal deficits result in accumulation of autophagic vacuoles engulfing damaged mitochondria along MN axons. Live imaging of spinal MNs from the adult disease mice demonstrates impaired dynein-driven retrograde transport of late endosomes (LEs). Expressing dynein-adaptor snapin reverses transport defects by competing with hSOD1^{G93A} for binding dynein, thus rescuing autophagy-lysosomal deficits, enhancing mitochondrial turnover, improving MN survival, and ameliorating the disease phenotype in hSOD1^{G93A} mice. Our study provides a new mechanistic link for hSOD1^{G93A}-mediated impairment of LE transport to autophagy-lysosomal deficits and mitochondrial pathology. Understanding these early pathological events benefits development of new therapeutic interventions for fALS-linked MN degeneration.

INTRODUCTION

Amyotrophic lateral sclerosis (ALS) is one of the most common adult-onset motor neuron (MN) degenerative disorders. About 10% of ALS cases are familial, of which over 20% are associated with dominant mutations in Cu/Zn superoxide dismutase (SOD1) genes (Rosen et al., 1993). Although the toxic mutant SOD1 gain of function is involved in the pathogenesis (Ilieva et al., 2009), multiple pathologic factors contribute to ALS-linked MN loss (Cleveland and Rothstein, 2001). However, early pathological changes occurring in spinal MNs far before the symptomatic stage remain obscure. Transgenic mice carrying mutant human SOD1 (hSOD1), especially hSOD1^{G93A}, are clinically and pathologically similar to human ALS patients (Gurney et al., 1994), thus serving as reliable familial ALS (fALS) models to understand the early pathological events.

Mitochondrial dysfunction, impaired dynamics, and degradation through mitophagy are associated with major neurodegenerative disorders (Chen and Chan, 2009; Sheng and Cai, 2012). Mutations in SOD1 and non-SOD1 ALS-related genes are associated with mitochondrial dysfunction (Cozzolino et al., 2013). Damaged mitochondria not only produce energy and buffer Ca^{2+} less efficiently than healthy ones, but also release harmful reactive oxygen species (ROS) and initiate apoptotic signaling cascades (Beal, 1996). Thus, mitochondrial pathology is a common state that triggers the decline of MN function and survival in ALS-linked pathogenesis. Proper clearance of those mitochondria via mitophagy in neurons may serve as an early protective mechanism, limiting the leakage of deleterious mediators from damaged mitochondria.

Altered mitochondrial transport was reported in fALS-linked hSOD1^{G93A}, TDP-43, and VAPB-P56S mice (Bilsland et al., 2010; De Vos et al., 2007; Magrané and Manfredi, 2009; Mórotz et al., 2012; Shan et al., 2010). Thus, one of the current hypotheses is that the aberrant axonal accumulation of damaged mitochondria could be due to reduced mitochondrial transport. We previously tested this hypothesis by genetically crossing fALS-linked hSOD1^{G93A} mice and *syntaphilin*$^{-/-}$ knockout mice. Syntaphilin acts as a docking receptor specifically targeting axonal mitochondria; deleting *syntaphilin* in mice results in the majority (~70%) of axonal mitochondria in a motile pool (Kang et al., 2008). We found that the 2-fold increase in axonal mitochondrial motility in the crossed hSOD1^{G93A}/*syntaphilin*$^{-/-}$ mouse does not slow ALS-like disease progression (Zhu and Sheng, 2011). Our findings are consistent with a recent study that mitochondrial transport deficits are not sufficient to cause axon degeneration in mutant hSOD1 models (Marinkovic et al., 2012), thus challenging the hypothesis that defective mitochondrial transport contributes to rapid-onset MN degeneration. These observations raise a fundamental question: does impaired degradation of damaged mitochondria through the lysosome system

play a more important pathological role during the early asymptomatic stage of fALS-linked mice?

Lysosomal maturation and function in neurons depend on the proper retrograde transport of late endosomes (LEs) and endolysosomal membrane trafficking (Cai et al., 2010; Lee et al., 2011); such transport and trafficking events are particularly challenging in spinal MNs with extended long axons. Our central hypothesis is that an imbalanced flux between autophagy or mitophagy induction and subsequent degradation within lysosomes will result in autophagic stress and mitochondrial pathology in axons, thus causing distal axons to become more vulnerable to dying-back degeneration. While the pathological roles of an impaired autophagy-lysosomal system in other neurodegenerative diseases were reported recently (Harris and Rubinsztein, 2012; Nixon, 2013), this cellular pathway was not examined in live spinal MN cultures isolated from disease-stage fALS-linked mouse models. Thus, it is very significant to investigate endolysosomal trafficking and autophagy-lysosomal maturation and degradation capacity in the context of both in vivo murine models and in vitro MNs isolated from adult mice.

In this study, we reveal MN-targeted progressive lysosomal defects in the hSOD1^{G93A} mice starting as early as postnatal day 40 (P40), accompanied by an aberrant accumulation of damaged mitochondria engulfed by autophagosomes in lumbar ventral root axons. These phenotypes were further confirmed in cultured spinal MNs, but not dorsal root ganglion (DRG) sensory neurons, isolated from young adult (P40) hSOD1^{G93A} mice. Our in vitro and in vivo studies demonstrate that endolysosomal transport is crucial to maintaining mitochondrial integrity and MN survival. Such deficits are attributable to impaired retrograde transport of LEs by mutant hSOD1^{G93A}, which interferes with dynein-snapin (motor-adaptor) coupling, thus reducing the recruitment of dynein motors to the organelles for transport. These deficits can be rescued by elevated snapin expression, which competes with hSOD1^{G93A} to restore dynein-driven transport. AAV9-snapin injection in hSOD1^{G93A} mice reverses mitochondrial pathology, reduces MN loss, and ameliorates the fALS-linked disease phenotype. Our study reveals a new cellular target for the development of early therapeutic intervention when MNs may still be salvageable.

RESULTS

Progressive Lysosomal Deficits in hSOD1^{G93A} MNs Starting at Asymptomatic Stages

Our previous study demonstrated that the hSOD1^{G93A} mouse strain (B6.Cg-Tg (SOD1^{G93A}) 1Gur/J) shows no MN loss until disease onset at P123–P127 and rapidly reaches disease end stage by P157 ± 9 (Zhu and Sheng, 2011). We asked whether spinal MNs display any detectable lysosomal deficits at early asymptomatic stages. We chose a lysosome-specific marker for our study. Antibodies against cathepsin D, a lysosomal aspartic protease, and LAMP-1 were used to co-immunostain lumbar spinal cords from P40 wild-type (WT) mice. In SMI32-labeled spinal MNs, almost all cathepsin D signals colocalized with LAMP-1, while a substantial number of LAMP-1 puncta were not labeled by cathepsin D, suggesting that cathepsin D is a reliable lysosome marker in MNs in vivo (Figure S1A). Strikingly, in P40 hSOD1^{G93A} mice, spinal MNs showed a substantially lower intensity of cathepsin D signals (Figures 1A and 1B). Quantitative analysis revealed a left shift in the distribution of hSOD1^{G93A} MNs to lower cathepsin D mean intensity relative to that from age-matched WT littermates (Figures 1C and 1D). With transmission electron microscopy (TEM), we observed a reduced density of morphologically featured lysosomes, characterized by electron-dense content, in the lumbar spinal MNs from P40 hSOD1^{G93A} mice (1.16 ± 0.14/100 μm^2, $p = 0.01$) compared to their WT littermates (1.68 ± 0.14/100 μm^2) (Figures 1E–1G). Thus, both light and electron microscopy images consistently suggest lysosomal deficits in hSOD1^{G93A} spinal MNs at an early asymptomatic stage.

To characterize lysosomal maturation and autophagic degradation in live MNs, we cultured spinal MNs isolated from adult diseased mice, combined with transgene expression. These cultured adult spinal MNs can be well maintained in vitro for up to 3 weeks (Figures S1B and S1C). Compared to embryonic MN cultures or cell lines routinely used in the ALS field, adult MN cultures provide more reliable cell models for investigating cellular mechanisms underlying adult-onset and spinal MN-targeted pathogenesis. First, we examined the relative density of cathepsin D in cultured spinal MNs at 7 days in vitro (DIV) isolated from adult (P40 or P65) WT and hSOD1^{G93A} mice. Cultured hSOD1^{G93A} MNs recapitulated lysosomal deficits shown in spinal MN slices (Figures 1H–1J), thus establishing a live MN model for studying adult-onset ALS-linked lysosomal deficits.

We confirmed the lysosomal deficits in cultured adult hSOD1^{G93A} MNs by examining mature forms of lysosomal cathepsin D and cathepsin B, which were specifically labeled by Bodipy FL-pepstatin A or the cresyl violet fluorogenic substrate CV-(Arg-Arg)2 (Magic Red), respectively. The majority of Bodipy FL-pepstatin A signals colocalized with cathepsin D in adult DRG neurons from P80 WT mice (Figure S1D). Some cathepsin D signals had low or no staining by Bodipy FL-pepstatin A, indicating immature lysosomes. In adult MN cultures from P40 hSOD1^{G93A} mice, normalized mean intensities of the active forms of cathepsins B and D were significantly reduced relative to that of WT littermates (Figures S1E–S1H), which is consistent in organotypic slice cultures of spinal cords from P40 hSOD1^{G93A} mice (data not shown), reflecting impaired lysosomal maturation at such an early asymptomatic stage.

Next, we asked whether lysosomal deficits become more robust with disease progression. We examined spinal MNs at various disease stages, including early asymptomatic (P21 and P40), presymptomatic (P80), disease onset (P120), and end stage (P148–P160). Mean intensity of cathepsin D in WT MNs was relatively stable between P21 and P40 and gradually increased after P80. Conversely, mean intensity of cathepsin D in hSOD1^{G93A} MNs progressively decreased to 81.7% ± 3.8% ($p < 0.001$) at P40, 73.0% ± 3.2% ($p < 0.001$) at P80, 35.5% ± 2.6% ($p < 0.001$) at P120, and 13.0% ± 3.5% ($p < 0.001$) at P148–P160 relative to that of aged-matched WT littermates (Figures 2A and 2B). It is notable that there were increased non-neuronal lysosomal signals at disease onset (P120) and end stage (P148–P160). This is likely attributable to glial lysosomal activation following glial proliferation (Wootz et al.,

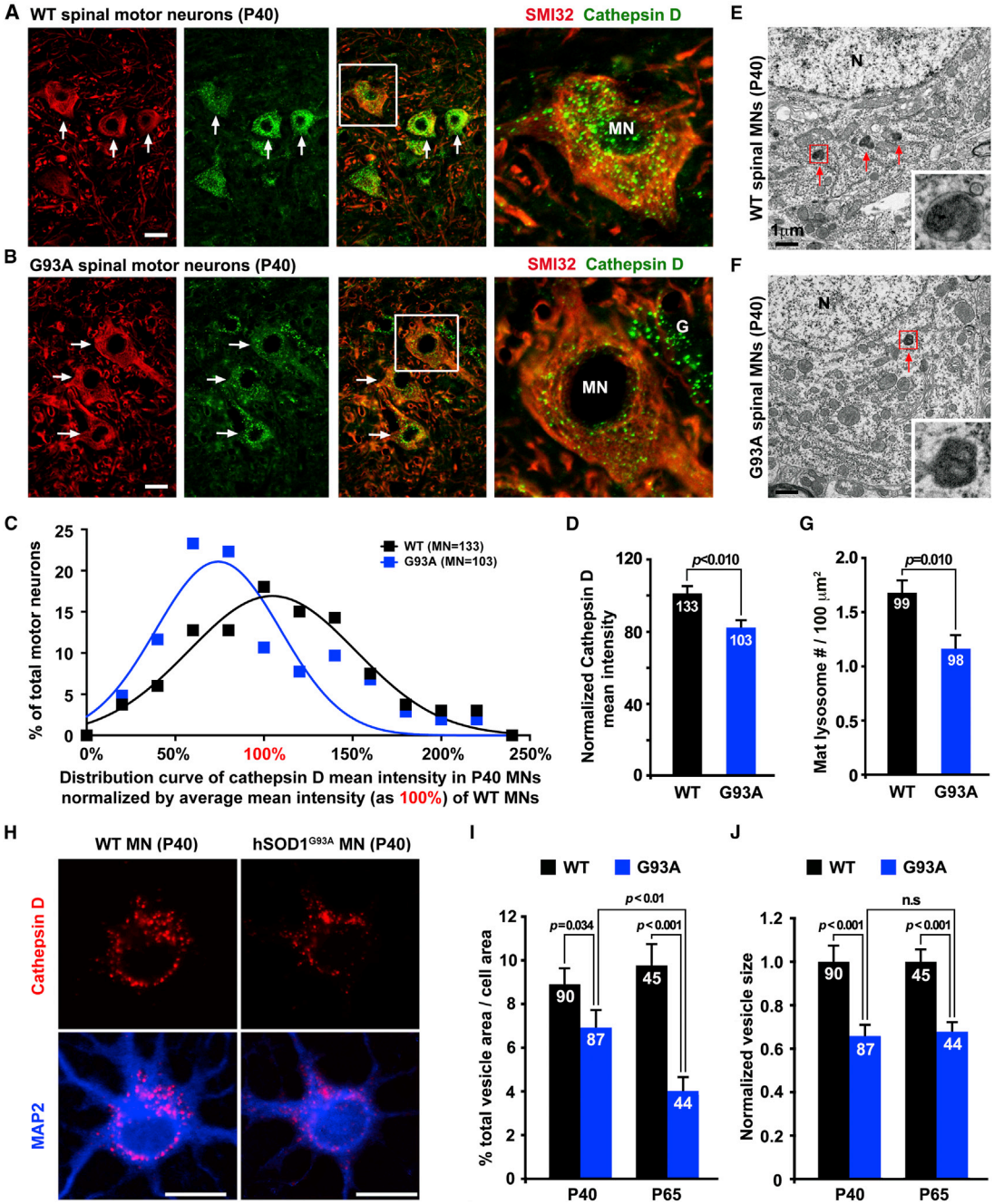

Figure 1. Reduced Lysosomal Density in Spinal MNs from Asymptomatic hSOD1^{G93A} Mice

(A–D) Images and quantitative analysis showing reduced lysosomal density in hSOD1^{G93A} MNs. Lumbar spinal cords from P40 WT (A) or hSOD1^{G93A} mice (B) were co-immunostained with MN marker SMI32 and lysosome marker cathepsin D. Arrows point to MNs. (A) and (B) show enlarged images (right panels) from boxed MNs. Integrated intensity of cathepsin D was measured using NIH ImageJ, followed by calibration with the size of the soma and expressed as mean intensity, which was normalized by the average mean intensity in WT MNs setting as 100% (D). There is a left shift in the distribution of cathepsin D mean intensity in hSOD1^{G93A} MNs (C). Data were collected from the total number of MNs (indicated within bars) from six WT and five hSOD^{G93A} littermates. G, glial cell.

(E–G) Electron micrographs (E and F) and quantitative analysis (G) showing reduced density of lysosomes with electron-dense contents (red arrows) in the spinal MNs of P40 hSOD1^{G93A} mice. Boxed area shows enlarged images of lysosomes. Data were analyzed from the total number of micrographs (indicated within bars) taken from three pairs of littermates. N, nucleus.

(H–J) Images (H) and quantitative analysis (I and J) showing reduced lysosomal mean intensity in cultured MNs isolated from adult (P40 and P65) hSOD1^{G93A} mice. Neurons were co-immunostained with cathepsin D and MAP2 at 7 DIV.

Scale bars, 20 μm (A, B, and H) and 1 μm (E and F). Data were analyzed from the total number of cultured MNs (indicated within bars) and expressed as mean ± SE with the Student's t test (also see Figure S1).

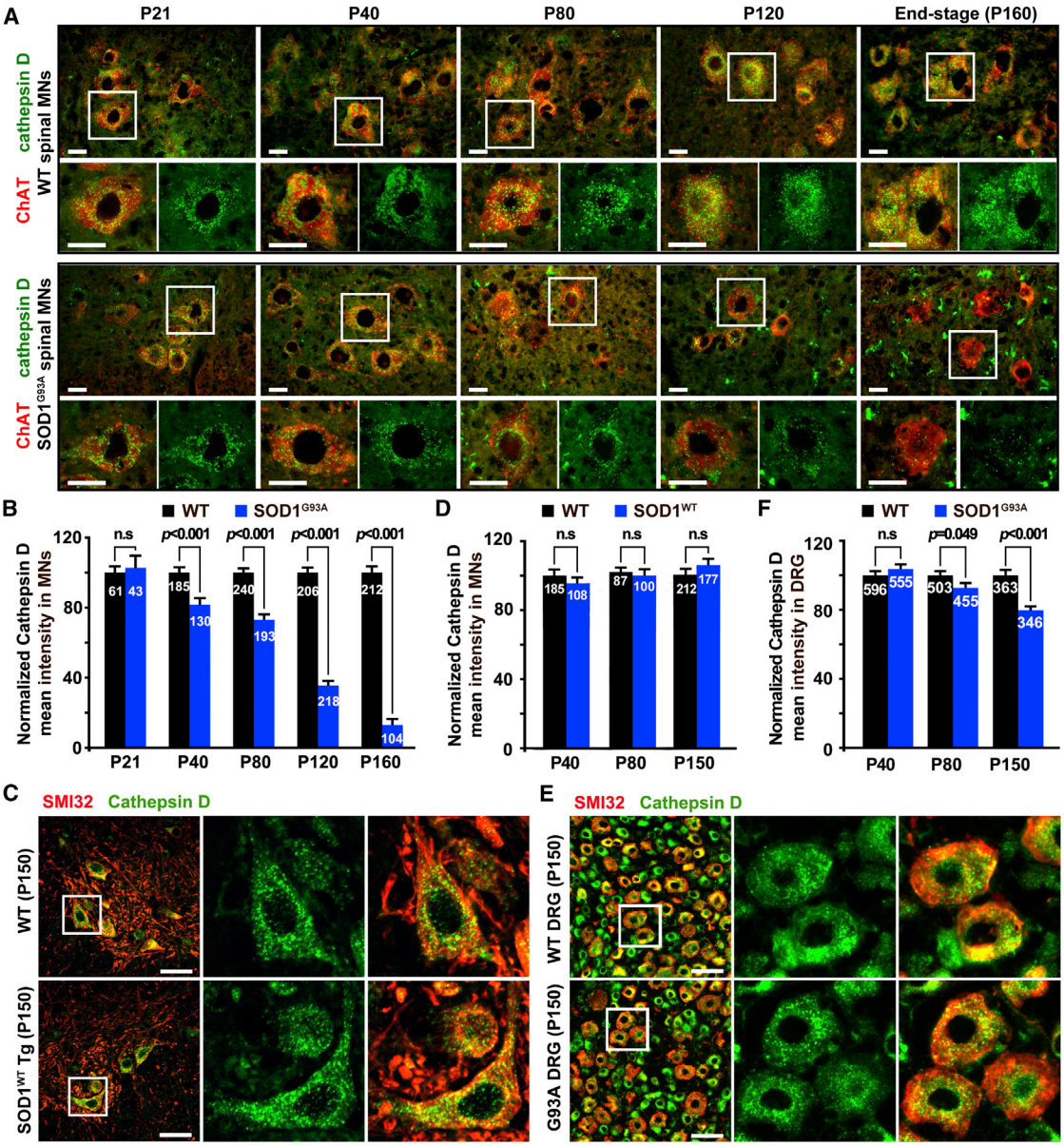

Figure 2. Progressive Lysosomal Deficits in hSOD1^{G93A} Spinal MNs

(A and B) Images (A) and quantitative analysis (B) show progressive reduction of lysosomal density in spinal MNs from early asymptomatic stage to the disease end stage. Lumbar spinal cords were co-stained with cathepsin D and the MN marker ChAT.

(C and D) Images (C) and quantitative analysis (D) show no reduction of cathepsin D intensity in WT hSOD1 mice at P150.

(E and F) Images (E) and quantitative analysis (F) show a slight reduction in lysosomal density in DRG neurons at late (P150) disease stages of hSOD1^{G93A} mice. Scale bars, 20 μm (A, C, and E). All data were expressed as mean ± SE with the Student's t test. At least three pairs of littermates were used for each time point and the total number of MNs for analysis is indicated within bars (B, D, and F) (also see Figure S2).

2006), which was evidenced by cathepsin D signals that were mainly localized in the GFAP-positive astrocytes or Iba1-positive microglia at the disease end stage (Figure S2A). As a control, the transgenic mice expressing WT hSOD1 displayed no lysosomal deficits as late as P150 (Figures 2C and 2D). We also examined DRG sensory neurons from the same mutant hSOD1^{G93A} mice. Normalized mean intensity of cathepsin D in DRG neurons was slightly reduced to 83.7% ± 1.7% of WT levels at the disease end stage (Figures 2E and 2F), a much milder reduction compared to that found in the mutant spinal MNs. There was no statistical difference in the matured forms of cathepsins B and D between WT and mutant DRG cultures from pre-symptomatic (P80) hSOD1^{G93A} mice (Figures S2B–S2E). Thus, progressive lysosomal deficit is an MN-targeted pathological event beginning at early asymptomatic stages in hSOD1^{G93A} mice.

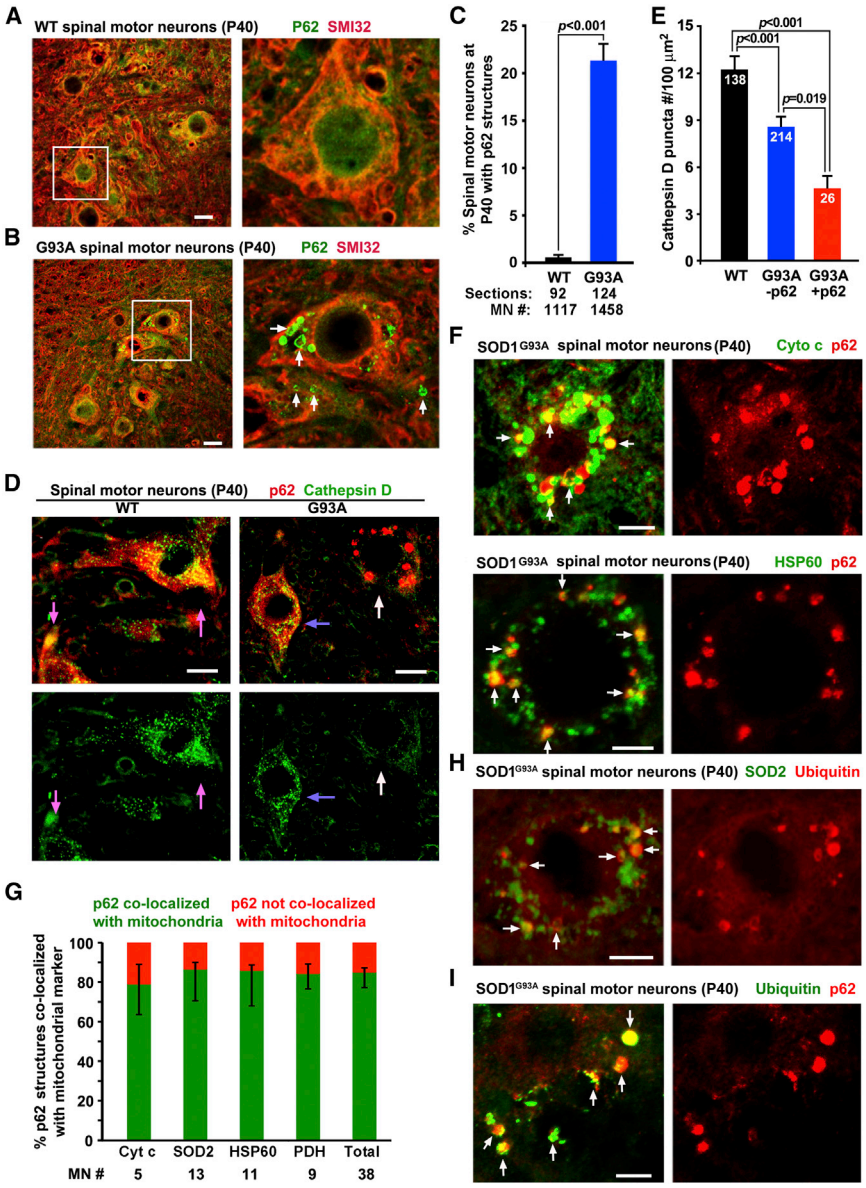

Figure 3. Lysosomal Deficits Associate with Accumulated AVs in Spinal MNs from Early Asymptomatic hSOD1^{G93A} Mice

(A–C) Images (A and B) and quantitative analysis (C) showing p62 ring-like AVs (arrows) in a population (21.35% ± 1.76%) of hSOD1^{G93A} spinal MNs. P40 lumbar spinal cord slices were co-stained with SMI32 and p62. (Right) Enlarged views of the boxed MNs are shown. Data were analyzed from a large number of MNs (n > 1,000) from the total number of slice sections (indicated below bars) taken from 19 WT and 14 hSOD1^{G93A} mice.

(D and E) Images (D) and quantitative analysis (E) showing the correlation of reduced cathepsin D density and accumulated p62 structures (white arrows) in P40 hSOD1^{G93A} MNs. Blue arrows point to mutant MNs with high cathepsin D density but no detectable large p62 structures. Pink arrows indicate WT neurons. Data were analyzed from the total number of MNs indicated within bars (E) taken from four pairs of littermates.

(F and G) Images (F) and quantitative analysis (G) show the colocalization of the majority of p62 structures (85.28%) with mitochondrial markers cytochrome *c* (Cyto *c*) or heat shock protein 60 (HSP60) in spinal MNs from P40 hSOD1^{G93A} mice (also see Figure S3).

(H and I) Representative images show ubiquitination of p62-targeted mitochondria in the spinal MNs from P40 hSOD1^{G93A} mice.

Scale bars, 20 μm (A, B, D, F, and H) and 10 μm (I). Data were expressed as mean ± SE with the Student's t test.

Impaired Autophagic Clearance Associates Mitochondrial Pathology in MN Axons

Our findings raise a question of whether robust lysosome deficits in the spinal MNs impair autophagic and mitophagic clearance. To address this issue, we examined lumbar spinal cord slice sections by co-immunostaining SMI32 and the autophagy marker p62. The p62 ring-like structures were accumulated in a population (21.35% ± 1.76%) of MNs from P40 hSOD1^{G93A} mice (Figures 3A–3C), but were rarely found in MNs from WT littermates (0.57% ± 0.26%, $p < 0.001$). This phenotype was reproduced in cultured spinal MNs at 7 DIV from P40 hSOD1^{G93A} mice (Figures S3A and S3B). Interestingly, MNs with large clustered p62 structures showed a more robust reduction in cathepsin D density relative to that from the mutant MNs with no detectable p62 puncta ($p = 0.019$) or from WT MNs ($p < 0.001$) (Figures 3D and 3E). Thus, the extent of lysosomal deficits correlates with levels of accumulated autophagic vacuoles (AVs). The majority (85.28%) of p62-labeled vacuoles in the mutant MNs colocalized with various mitochondrial markers (Figure 3G), including cytochrome *c* (Cyto *c*), heat shock protein 60 (HSP60) (Figure 3F), superoxide dismutase 2 (SOD2), or pyruvate dehydrogenase (PDH) (Figures S3C and S3D), representing mitophagic intermediates engulfing damaged mitochondria, some of which show ubiquitination (Figures 3H and 3I). Aberrant clustering of P62-labeled mitochondria in hSOD1^{G93A} MNs supports our hypothesis that lysosomal deficits impair degradation of damaged mitochondria.

We examined mitochondrial ultrastructures in lumbar spinal cords and ventral root axons. Although swollen and vacuolated mitochondria were observed in hSOD1^{G93A} MN soma (Figure S4A), mitochondria in ventral root axons displayed more robust degenerative phenotypes, including fragmentation, cristae distortions, vacuolization, or swelling and clustering (Figures 4A and 4D). These phenotypes were readily detectable as early as P40 in hSOD1^{G93A} mice, but rarely found in WT littermates. Quantitative analysis revealed reduced mitochondrial density in the soma of spinal MNs and relatively increased

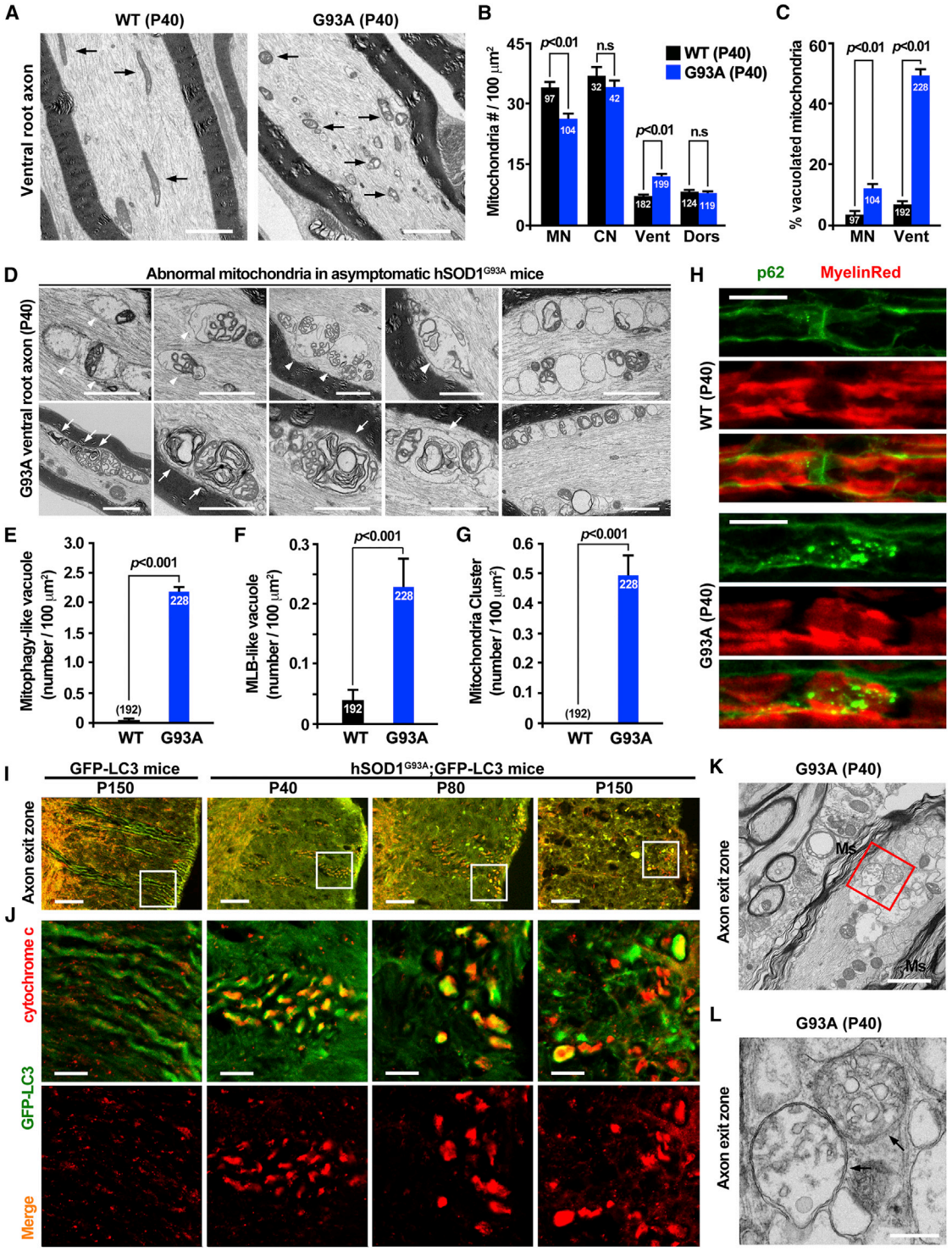

Figure 4. Mitochondrial Pathology in the Ventral Root Axons of Early Asymptomatic hSOD1^{G93A} Mice

(A–C) Electron micrographs and quantification show fragmented, vacuolated, and clustered mitochondria (A); increased mitochondrial density (B); and robustly increased vacuolated mitochondria (C) in the ventral root axons (Vent) of early asymptomatic hSOD1^{G93A}.

(D–G) Electron micrographs (D) and quantification (E–G) show an accumulation of AVs engulfing damaged mitochondria (arrowheads) and multilamellar bodies (MLBs, arrows) in lumbar ventral root axons from P40 hSOD1^{G93A} mice. Note that clustered mitochondria (right) were found at this early age.

(H) Clustering of p62 AVs in ventral root axons from P40 hSOD1^{G93A} mice. Axon myelin sheaths are outlined with MyelinRed.

(legend continued on next page)

density in the ventral root axons ($p < 0.01$) (Figure 4B). No significant change was observed in mitochondrial density in cortical MNs and dorsal root axons between P40 WT and hSOD1^{G93A} littermates. Only mild mitochondrial vacuolization was seen in mutant dorsal root axons (Figure S4A). Mitochondrial vacuolation was more robust in ventral root axons (49.90% ± 2.07%) compared to the soma of MNs (12.12% ± 0.94%) from the same P40 hSOD1^{G93A} mice (Figures 4C and 4D). Mitochondrial clustering was further confirmed in ventral root slice sections by staining axonal mitochondrial marker syntaphilin (Figure S4B).

In addition to altered mitochondrial ultrastructure, we observed more striking axonal phenotypes in hSOD1^{G93A} mice as follows: aberrant accumulation and clustering of multilamellar bodies (MLBs) and amphisome-like structures engulfing damaged mitochondria with collapsed cristae (Figures 4D–4G). These unique structures were readily found in ventral root axons of P40 hSOD1^{G93A} mice, but were almost absent in age-matched WT mice. MLBs are altered autolysosomes containing multiple concentric membrane layers and are associated with various lysosomal storage diseases (Hariri et al., 2000), while amphisomes are intermediate AVs originating from the fusion between late endocytic vacuoles and autophagosomes (Cheng et al., 2015). These MLBs and amphisomes also were enriched in cortical neurons by inhibiting lysosomal cathepsin D proteolysis (Boland et al., 2008). Furthermore, we crossed the GFP-LC3 transgenic mouse (Mizushima et al., 2004) with the hSOD1^{G93A} mouse. Colocalization of mitochondria and GFP-LC3-labeled AVs was readily detectable within axon exit zones in the crossed mutant mice (Figures 4I and 4J). TEM analysis confirmed that double-membrane AV-like structures engulfing damaged mitochondria and other degradative materials were clustered within the axon exit zones (Figures 4K and 4L). Consistently, p62-labeled AVs were clustered along ventral root axons of P40 hSOD1^{G93A} mice, but rarely in the age-matched WT (Figure 4H). Thus, our study suggests impaired autophagy-mitophagy degradation in MN axons of hSOD1^{G93A} mice at early asymptomatic stages.

Snapin Rescues LE Retrograde Transport by Competing with hSOD1^{G93A} for Binding to Dynein

Lysosomal maturation in neurons depends on proper LE retrograde transport and endolysosomal trafficking (Cai et al., 2010; Lee et al., 2011), which is driven by dynein motors from distal processes to the soma. Our findings raise the question of whether lysosomal deficits in hSOD1^{G93A} MNs reflect altered endolysosomal trafficking. To address this issue, we took advantage of live spinal MN cultures from P40 mice to examine axonal transport of late endocytic organelles labeled with GFP-Rab7 (see Experimental Procedures). In WT MNs, LEs appeared as small fine vesicular structures distributed evenly along processes. In contrast, they were clustered in larger puncta in processes of mutant MNs (Figure 5A). Time-lapse imaging showed predominant retrograde transport of LEs along processes toward the soma in WT MNs (Figures 5B and 5C). However, hSOD1^{G93A} MNs displayed reduced retrograde transport ($p = 0.03$), while there was no significant change in anterograde transport ($p > 0.05$).

Snapin acts as an adaptor recruiting dynein motors to LEs via binding to the dynein intermediate chain (DIC), thus coordinating dynein-driven retrograde transport and endolysosomal trafficking (Cai et al., 2010). LE-loaded dynein-snapin complexes drive AV retrograde transport after they fuse into amphisomes (Cheng et al., 2015). These mechanisms enable neurons to maintain efficient degradation capacity. To rescue lysosomal deficits and mitochondrial pathology, we introduced the *snapin* transgene into mutant hSOD1^{G93A} MNs through lentivirus infection. Elevated snapin expression enhanced retrograde ($p < 0.001$), but not anterograde, transport of LEs (Figures 5D and 5E) and reduced their clustering in the processes of mutant MNs (Figure 5A). As a control, expressing the snapin^{L99K} mutant defective in DIC binding failed to rescue the retrograde transport (Figures S5A and S5B), further confirming the role of snapin-DIC coupling in driving LE transport.

It was reported that mutant hSOD1^{G93A}, but not WT hSOD1, interacts with the DIC (Zhang et al., 2007). This raises the question of whether the mutant hSOD1 competes with snapin for binding the DIC, thus interfering with the snapin-DIC coupling in recruiting dynein to LEs for retrograde transport (Figure 5I). To address this question, we immuno-isolated late endocytic organelles from spinal cords with Dynal magnetic beads coated with an anti-Rab7 antibody. Association of the DIC with Rab7-labeled organelles was reduced to 34% in P40 hSOD1^{G93A} mice compared to that from age-matched WT mice ($p < 0.001$) (Figures 5F and 5G). This reduced DIC tethering to Rab7-labeled organelles was not observed in hSOD1^{wt} transgenic mice (Figures S5C and S5D). We further showed that the DIC selectively binds to hSOD1^{G93A}, but not hSOD1^{wt} (Figure 5H). While snapin binds to the DIC, but not to hSOD1^{WT} and hSOD1^{G93A} under the same conditions (Figure S5E), overexpressing snapin inhibited hSOD1^{G93A}-DIC coupling (Figure 5H). These data support our hypothesis that retrograde transport of LEs is impaired by hSOD1^{G93A}-DIC interaction, which interferes with the snapin-DIC complex, thereby reducing dynein recruitment to LEs for transport (Figures 5F and 5I). By competitively binding to the DIC, hSOD1^{G93A} and snapin play opposite roles in dynein-driven LE retrograde transport.

Impaired Retrograde Transport Underlying Lysosomal Deficits

We thought to ask whether enhancing retrograde transport by snapin could rescue autophagy-lysosomal deficits in vivo and in vitro. First, we overexpressed snapin in the spinal cord of hSOD1^{G93A} mice by injecting AAV9-mChery-P2A-snapin into P0

(I and J) Aberrant accumulation of LC3-labeled AVs engulfing fragmented mitochondria (cytochrome *c*) in axon exit zones of crossed GFP-LC3/hSOD1^{G93A} mice at P40, P80, and P150 stages. (J) shows zoomed images of the boxed area in (I).

(K and L) Electron micrographs showing clustered AVs (arrows) engulfing organelles in the axon exit zone of P40 hSOD1^{G93A} mice. The red box was enlarged in (L). Ms, myelin sheath.

Data were analyzed from a total number of micrographs indicated within bars (B, C, and E–G) and expressed as mean ± SE with the Student's t test. Scale bars, 2 μm (A, D, and K), 20 μm (H and I), 5 μm (J), and 500 nm (L) (also see Figure S4).

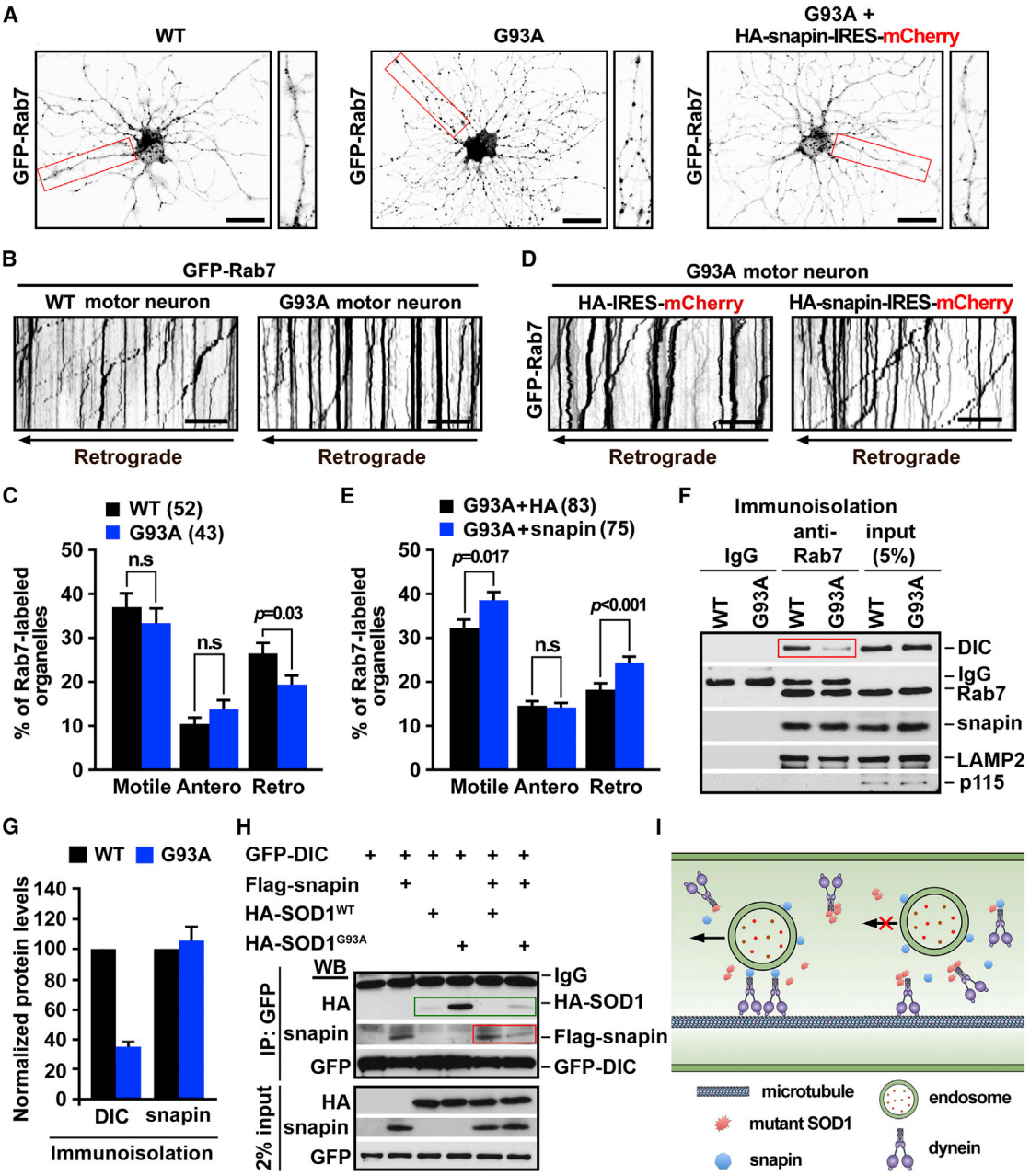

Figure 5. Snapin Rescues LE Retrograde Transport by Competing with hSOD1^{G93A} for Binding to Dynein

(A) Images showing distribution of Rab7-labeled organelles in adult spinal MNs from P40 WT or hSOD1^{G93A} mice. Note that LEs in the mutant MNs appeared as large clusters along processes. Transient snapin overexpression reversed the mutant phenotype (right). Neurites in red boxes were zoomed on the right side.

(B and C) Kymographs (B) and quantitative analysis (C) showing reduced LE retrograde transport in P40 hSOD1^{G93A} MNs. Time-lapse imaging was recorded at 7 DIV for 100 frames with 2.5-s intervals. In kymographs, vertical lines represent stationary organelles; oblique lines or curves to the left indicate retrograde transport.

(D and E) Kymographs (D) and quantitative analysis (E) showing enhanced LE retrograde transport by expressing *snapin* transgene in hSOD1^{G93A} MNs. Motility was quantified from the total number of neurites as indicated in parentheses from three experiments and expressed as mean ± SE with Student's t test. Scale bars, 20 μm (A, B, and D).

(F and G) Immuno-isolation (F) and quantitative analysis (G) showing reduced association of the DIC with LEs in hSOD1^{G93A} mouse spinal cords. Data were analyzed from three repeats and expressed as mean ± SE.

(H) Immunoprecipitation showing competitive binding of snapin and hSOD1^{G93A} with the DIC. Note that snapin inhibits the hSOD1^{G93A}-DIC coupling (green box), while hSOD1^{G93A}, but not hSOD1^{wt}, reduced the snapin-DIC coupling (red box).

(I) Proposed model: snapin serves as an adaptor attaching dynein to LEs through binding to the DIC (left). In hSOD1^{G93A} MNs, the snapin-DIC coupling is blocked by the hSOD^{G93A}-DIC interaction (right), thus impairing LE retrograde transport. Elevated snapin expression reverses the mutant phenotype by competing with hSOD1^{G93A} for binding the DIC (also see Figure S5).

mice through the temporal vein, an established in vivo MN gene delivery procedure (Foust et al., 2010). The majority (>96%) of SMI32- or NeuN-labeled spinal MNs in P40 mice were infected (Figures S6A–S6D). There was a significant increase in cathepsin D mean intensity in both WT and hSOD1^{G93A} spinal MNs of P40 mice after in vivo snapin overexpression (Figures 6A and 6B). Consistently, quantitative analysis of TEM micrographs (>164 for each) revealed an increased density of morphologically featured lysosomes in hSOD1^{G93A} spinal cords following in vivo snapin overexpression (Figures 6C and 6D). In addition, transient HA-snapin expression in cultured P40 hSOD1^{G93A} MNs significantly increased mean intensity (31.59%, $p = 0.001$) and density (47.11%, $p < 0.001$) of Bodipy FL-pepstatin A-labeled mature lysosomes relative to that from the same mutant MNs expressing HA control (Figures 6E–6G).

Next we asked whether rescuing lysosomal deficits by expressing snapin in MNs is sufficient to enhance autophagic degradation capacity. First, we infected cultured adult MNs with Lenti-mRFP-GFP-LC3, a chimeric LC3 autophagy reporter tagged to both GFP (acid sensitive) and mRFP (acid stable), followed by live imaging GFP versus mRFP signals. An autophagosome acquires acidic properties when it matures into an autolysosome. In WT neurons, GFP, but not mRFP, was degraded rapidly in mature acidic autolysosomes (Figure 6H, top). In contrast, lysosomal deficits in hSOD1^{G93A} MNs resulted in the accumulation of immature AVs, within which both GFP and mRFP signals were retained (Figure 6H, middle). Mander's coefficient analysis showed an enhanced colocalization ratio of mRFP and GFP signals in the mutant MNs from early asymptomatic mice (P40) (Figure 6I), indicating an impaired autophagic maturation or clearance. Snapin expression fully reversed the mutant phenotype: GFP underwent rapid degradation (Figures 6H, bottom). Second, we examined p62-labeled AVs in the infected spinal cords of P40 hSOD1^{G93A} mice. Elevated snapin expression significantly reduced the percentage of MNs displaying AV-like structures (Figures 6J and 6K). The rescued phenotype was further confirmed in cultured mutant MNs (Figures S6E and S6F), indicating enhanced autophagic clearance following snapin overexpression. To provide a mechanistic link between rescued lysosomal deficits and enhanced dynein-driven LE retrograde transport, we expressed snapin^{L99K} mutant defective in DIC binding in P40 hSOD1^{G93A} MNs. In contrast to the effective rescue capacity by expressing WT snapin, expressing snapin^{L99K} mutant failed to enhance active cathepsin D levels (Figures S6G and S6H), failed to reduce p62-labled AVs (Figure S6I), and further impaired degradation of GFP in adult hSOD1^{G93A} MNs (Figure S6J). Thus, early deficits in autophagy-lysosomal function in hSOD1^{G93A} MNs can be rescued effectively by snapin expression both in vitro and in vivo. Elevated snapin competes with hSOD1^{G93A} for binding to dynein motors, thereby enhancing endolysosomal trafficking and maturation.

Enhanced Retrograde Transport Reverses Mitochondrial Pathology and Reduces Disease Progression in hSOD1^{G93A} Mice

The sequestration of damaged mitochondria into autophagosomes and subsequent degradation within lysosomes constitute a key cellular pathway in maintaining mitochondrial quality. We proposed that snapin-mediated enhancement of autophagy-lysosomal function in hSOD1^{G93A} MNs facilitates the removal of damaged mitochondria. To test our hypothesis, we examined mitochondrial ultrastructure in ventral root axons from P40 WT and hSOD1^{G93A} mice injected with AAV9-snapin or AAV9 control vector. The robust mitochondrial degeneration, including fragmentation, cristae distortions, vacuolization, swelling, and clustering, that was observed in P40 hSOD1^{G93A} mice (Figures 4A and 4D) was significantly reduced following injection with AAV9-snapin, but remained in mutant mice injected with control AAV9 vector (Figures 7A–7C). In addition, snapin overexpression dramatically reduced the number of MLBs in hSOD1^{G93A} mice axons (Figure 7D). Since those MLBs likely originated from degenerative mitochondria (Figure 4D), these in vivo rescue effects support our notion that elevated snapin expression plays a crucial role in reducing mitochondrial pathology by removing damaged mitochondria in the diseased MN axons.

We further examined axonal mitochondrial membrane potential ($\Delta\psi_m$) and free radical generation, two parameters widely used to assess mitochondrial integrity. First, by loading live MNs at 14 DIV with the fluorescent dye TMRE, which stains mitochondria depending on $\Delta\psi_m$, we found a significant decrease ($p < 0.001$) in TMRE mean intensity in axonal mitochondria from adult hSOD1^{G93A} MNs compared to those from age-matched WT MNs (Figure 7E), indicating mitochondrial depolarization. Transient snapin expression restored mitochondrial $\Delta\psi_m$. Second, we examined superoxide levels in axonal mitochondria with MitoSOX Red, a mitochondrion-specific superoxide indicator. Parallel imaging of superoxide levels demonstrated elevated ROS production ($p < 0.001$) in axonal mitochondria from P40 hSOD1^{G93A} MNs relative to WT MNs, a phenotype that could be suppressed by snapin overexpression (Figure 7F). These two experiments further support our hypothesis that enhancing autophagy-lysosomal activity by expressing snapin removes damaged mitochondria from axons.

We conducted three lines of in vivo and in vitro experiments to examine whether expressing snapin has any beneficial impact on MN survival and disease progression in hSOD1^{G93A} mice. First, we examined MN loss in lumbar spinal cords following viral injection. At the early asymptomatic age (P40), no significant difference was detected in the spinal cord MN counts between WT and hSOD1^{G93A} mice ($p > 0.05$) (Figure 7G). When animals reached the disease end stage (P150), there was a significant reduction in MN number in hSOD1^{G93A} mice injected with the AAV9 control vector ($p < 0.001$) compared with aged-matched WT mice (Figure 7H). However, such MN loss was reduced following in vivo snapin overexpression in spinal cords ($p < 0.01$). Next, we examined MN survival by performing terminal deoxynucleotidyl transferase dUTP nick end-labeling (TUNEL) assays. In cultured P40 hSOD1^{G93A} MNs at 14 DIV, 15.83% of MNs were TUNEL positive, higher than age-matched WT MNs ($p < 0.05$) (Figure S7A). Snapin overexpression reduced the apoptosis rate to 6.51% ($p < 0.01$). Consistently, P40 hSOD1^{G93A} MN cultures showed reduced survival rates relative to age-matched WT MNs; snapin overexpression increased survival over time. At 14 DIV, hSOD1^{G93A} MNs expressing HA control

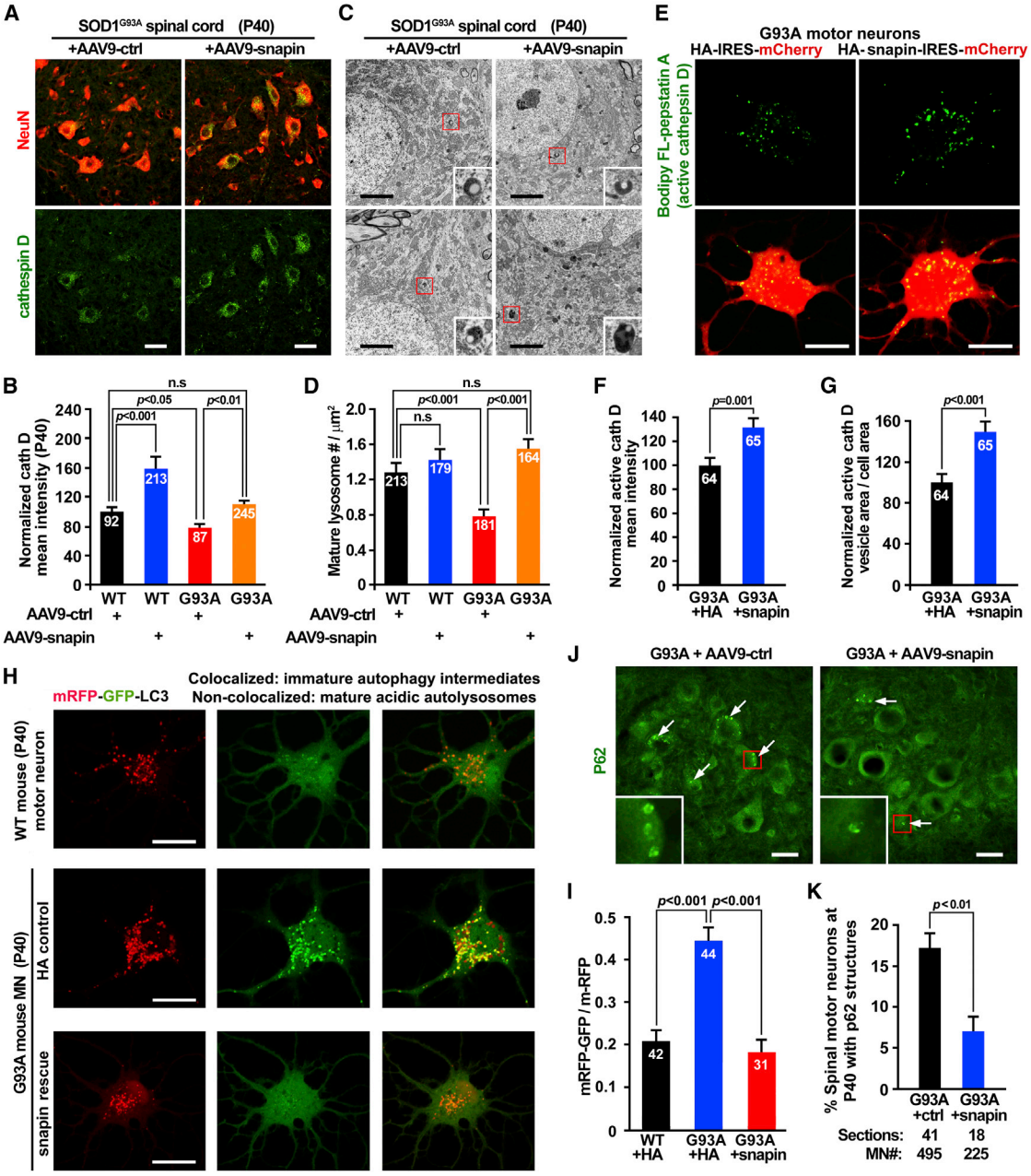

Figure 6. Enhancing Retrograde Transport by Snapin Rescues Autophagy-Lysosomal Deficits

(A and B) Images (A) and quantitative analysis (B) showing rescued lysosomal deficits in hSOD1^{G93A} MNs following AAV9-snapin infection. Lumbar spinal cords from P40 mice were co-immunostained with NeuN and cathepsin D.

(C and D) Electron micrographs (C) and quantitative analysis (D) showing increased density of lysosomes with electron-dense content in the spinal MNs of P40 hSOD1^{G93A} mice after snapin overexpression. Boxed area shows enlarged images of lysosomes.

(E–G) Images (E) and quantitative analysis (F and G) show increased intensity and density of active cathepsin D labeled by Bodipy FL-pepstatin A following snapin transient expression in adult MN cultures of P40 hSOD1^{G93A} mice.

(H and I) Images (H) and quantitative analysis (I) showing that snapin rescued autophagic flux in adult hSOD1^{G93A} MNs. MNs were co-infected with Lenti-mRFP-GFP-LC3 and HA-snapin or HA control virus. GFP, but not mRFP, was rapidly degraded in mature acidic lysosomes. Mander's coefficient reflects the relative ratio of colocalization between mRFP and GFP signals (I).

(J and K) Images (J) and quantitative analysis (K) showing reduced P62 autophagic structures in the spinal MNs of P40 hSOD1^{G93A} mice following AAV9-snapin infection. Boxed area shows enlarged images of P62 ring-like structures.

Data were analyzed from the total number of MNs (B, F, G, I, and K) or micrographs (D) (indicated within bars) taken from three pairs of mice (D) or in three independent experiments, and expressed as mean ± SE with the Student's t test. Scale bars, 20 μm (A, E, H, and J) or 2 μm (C) (also see Figure S6).

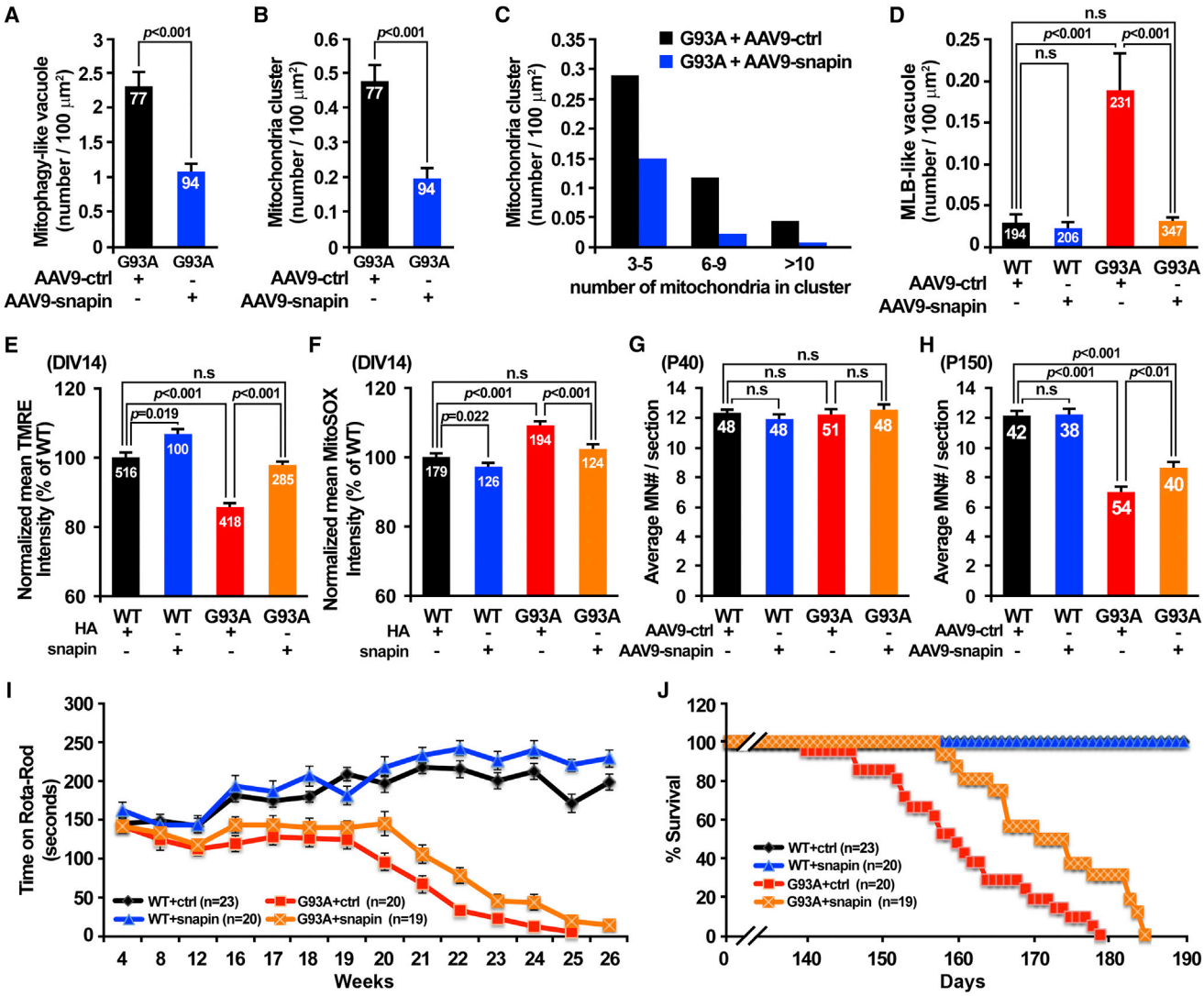

Figure 7. Snapin Reduces Mitochondrial Pathology and Delays Disease Progression

(A–D) AAV9-snapin infection in hSOD1^{G93A} mouse spinal cords significantly reduced the density of degenerated mitochondria with >50% loss of cristae (A), removed clusters of damaged mitochondria (B and C), and facilitated clearance of MLBs (D).

(E) Elevated snapin expression reversed depolarized ($\Delta\psi_m$) axonal mitochondrial phenotype in the mutant MNs. MNs at 1 DIV were infected with pLenti-snapin-IRES-GFP or pLenti-HA-IRES-GFP control, followed by loading (20 nM, 15 min) of $\Delta\psi_m$-dependent fluorescent dye TMRE at 14 DIV.

(F) Elevated snapin expression reduced mitochondrial oxidative stress in the mutant MNs. Note that axonal mitochondria in hSOD1^{G93A} MNs displayed elevated superoxide fluorescence, which was reversed by snapin overexpression.

(G and H) In vivo snapin expression significantly increased MN survival in hSOD1^{G93A} mice at disease end stage.

(I) Rota-rod tests detected increased time remained on rota-rod in hSOD1^{G93A} mice injected with AAV9-snapin. Each mouse was placed on an accelerated rod with speed from 5 to 40 rpm over 3 min. The latency to fall off the rota-rod was recorded.

(J) Elevated in vivo snapin expression extended the lifespan of hSOD1^{G93A} mice. Note that death initiation in hSOD1^{G93A} mice was postponed from P140 in AAV9 control group to P158 in AAV9-snapin group. The average lifespan of hSOD1^{G93A} mice increased to 173 ± 10 days with AAV9-snapin injection, compared to 161 ± 11 days in the AAV9 control group.

Data were analyzed from the total number of micrographs (A–D), MNs (E and F), or spinal cord slices (G and H) indicated within bars in three to six independent experiments. Animal numbers are indicated within figures (I and J). Data are expressed as mean ± SE with Student's t test (also see Figure S7).

displayed a lower survival rate (36.18% ± 5.54%). However, snapin overexpression significantly enhanced survival of the diseased MNs (75.97% ± 10.22%, $p < 0.001$) (Figure S7B). Expressing snapin^{L99K}, a snapin mutant defective in DIC binding, had no beneficial impact on MN survival (39.48% ± 4.79%, $p = 0.66$) (Figure S7C). In contrast, this mutant reduced WT MN survival, likely through its dominant-negative effect on endogenous snapin.

We evaluated ALS-like disease onset and progression in hSOD1^{G93A} mice following AAV9-snapin injection. We weighed

the animals and tested motor coordination monthly during the first 3 months of age and then weekly after that. While WT mice continued to grow with age, snapin overexpression slightly reduced body weight in both female (~5%) and male (~10%) WT mice at 26 weeks old (Figures S7D and S7E). However, both male and female hSOD1^{G93A} mice began to lose weight at age 17–18 weeks; such weight loss was not affected by snapin overexpression. Rota-rod tests detected increased time remained on rota-rod in hSOD1^{G93A} mice injected with AAV9-snapin, indicating improved motor coordination after disease onset (Figure 7I). Notably, the initiation of death in hSOD1^{G93A} mice was postponed from P140 in the control group to P158 in the AAV9-snapin group. The average lifespan of hSOD1^{G93A} mice increased to 173 ± 10 days with AAV9-snapin injection, compared to 161 ± 11 days in the AAV9-control group (Figure 7J). WT mice with AAV9-snapin injection stayed alive throughout the duration of the experiment. Overall, reversing lysosomal deficits in hSOD1^{G93A} mice by in vivo snapin overexpression in spinal cords delayed disease progression.

DISCUSSION

In this study, we revealed for the first time that spinal MN-targeted progressive lysosomal deficits start as early as at P40 asymptomatic stages in fALS-linked hSOD1^{G93A} mice. These deficits impair autophagic/mitophagic degradation, thus resulting in an aberrant accumulation of AVs engulfing damaged mitochondria along ventral root axons. These pathological phenotypes were captured in cultured adult (P40) spinal MNs, but not in DRG sensory neurons from the same hSOD1^{G93A} mice. Such early deficits are due to reduced LE retrograde transport via competitive binding of hSOD1^{G93A} to the DIC, and they could be reversed by introducing *snapin* transgene in MNs. Snapin competes with hSOD1^{G93A} for binding to the DIC, thereby recruiting dynein to LEs for retrograde transport. Thus, snapin and hSOD1^{G93A} play opposite roles in LE retrograde transport. Furthermore, we showed that expressing snapin efficiently reverses autophagy-lysosomal deficits and facilitates the removal of damaged mitochondria, thereby prolonging mutant MN survival. Injecting AAV9-snapin into the diseased mice rescued lysosomal deficits in MNs in vivo and slowed MN degeneration and disease progression. Thus, our study advances our understanding of early pathological mechanisms underlying MN degeneration and also provides new mechanistic insights into the following: (1) how mutant hSOD1 impairs LE retrograde transport by interfering with motor-adaptor coupling, thus reducing dynein-cargo attachment; and (2) how elevated snapin expression reverses the mutant phenotypes by competing with hSOD1^{G93A} for dynein-driven retrograde transport (Figure 5I).

Lysosomal Deficit Is an Early Pathological Phenotype in hSOD1^{G93A} Mouse MNs

We revealed progressive lysosomal deficits in hSOD1^{G93A} spinal MNs with disease progression. There are three notable features in our observations as follows: (1) lysosomal deficits are MN targeted; (2) lysosomal deficits can be detected in mutant MNs from as early as P40 asymptomatic hSOD1^{G93A} mice, and become progressively worse after disease onset at P120 when MN loss was reported in hSOD1^{G93A} mice (Lambrechts et al., 2003); and (3) these lysosomal deficits are not observed in WT hSOD1 transgenic mice even as late as P150. These restricted and progressive changes highlight a mechanistic link between lysosome deficits and fALS-linked pathogenesis in spinal MNs. The increased cathepsin D signals restricted in glial cells after disease onset in hSOD1^{G93A} mice (Figures 2A and S2A) may reflect lysosomal activation following glial cell proliferation in the spinal cords.

Lysosomal Deficits Augment Mitochondrial Pathology

Autophagic flux is the equilibrium balance between autophagic formation and clearance. Since neurons are particularly sensitive to the accumulation of misfolded proteins and damaged organelles, newly formed autophagosomes are eliminated quickly by fusing with endolysosomes, thereby avoiding a buildup of AVs (Maday et al., 2012; Cheng et al., 2015). However, AVs accumulate rapidly in neurons when lysosomal proteolysis is inhibited (Lee et al., 2011). Impaired autophagic clearance also was reported in various lysosomal storage disorders (Kiselyov et al., 2007; Settembre et al., 2008). The accumulation of dysfunctional mitochondria is associated with a primary lysosomal defect in a mouse model of neuropathic Gaucher disease, an inherited lysosomal storage disorder (Osellame and Duchen, 2014). Thus, an imbalanced autophagic flux between enhanced autophagy/mitophagic induction and reduced clearance due to lysosomal deficits results in autophagic stress characterized by accumulated AVs engulfing protein aggregates and damaged organelles, such as mitochondria.

Altered autophagy was reported in fALS-linked mouse models. Autophagy receptor p62 colocalizes with hSOD1^{G93A} in fALS mouse spinal MNs (Gal et al., 2007) and interacts with mutant hSOD1^{G93A}, but not WT hSOD1^{WT}. Overexpressing p62 facilitates engulfing hSOD1^{G93A} aggregates into autophagosomes for degradation. This is consistent with our findings showing the p62 ring-like structures accumulated in MNs from P40 hSOD1^{G93A} mice (Figures 3A–3C). Interestingly, MNs with large p62 structures showed more robust lysosomal deficits (Figures 3D and 3E), thus impairing AV clearance. Our study suggests that early lysosomal deficits in hSOD1^{G93A} MNs lead to autophagic defects. Because mitochondrial pathology is a robust hallmark in fALS-linked MNs at asymptomatic stages, we assessed snapin rescue effects in both in vitro and in vivo hSOD1^{G93A} mouse models by focusing on mitochondrial pathology phenotypes, including ultrastructural changes, mitochondrial membrane potential ($\Delta\psi_m$), and free radical generation.

Although increased numbers of autophagosomes were observed in the spinal cords of sALS patients and hSOD1^{G93A} mice during late disease stages (Li et al., 2008; Morimoto et al., 2007), the contribution of altered autophagy to the fALS-linked pathogenesis has been a subject of debate. It remains unclear whether enhanced induction of autophagy helps remove toxic mutant protein aggregates or instead facilitates MN degeneration. In vivo treatment of hSOD1^{G93A} mice with rapamycin, an autophagy inducer via the mTOR-signaling pathway, augmented MN degeneration and disease progression and failed to reduce mutant hSOD1 aggregates in the spinal cords (Zhang et al., 2011). However, inducing mTOR-independent autophagy in

hSOD1^{G93A} mice prolonged their lifespan and attenuated the progression of disease phenotypes (Castillo et al., 2013). Studies using lithium, an mTOR-independent autophagy inducer (Sarkar et al., 2005), reported controversial results in the same hSOD1^{G93A} mice. While one study showed that activating autophagy reduced MN loss in hSOD1^{G93A} mice (Fornai et al., 2008), two studies found that it caused an earlier onset of the disease and a reduced lifespan (Gill et al., 2009; Pizzasegola et al., 2009). Clinical trials by administering therapeutic doses of lithium showed no effect in ALS patients (Chiò et al., 2010).

These controversial findings raise a question of whether the observed AVs in fALS-linked spinal MNs reflect enhanced autophagy induction or impaired autophagic clearance. Addressing this question is critical for future therapeutic strategies for ALS clinical trials. Our study provides in vitro and in vivo evidence that progressive lysosomal deficits combined with impaired degradation of damaged mitochondria are the early pathological events in hSOD1^{G93A} spinal MNs. The striking AV accumulation in ventral root axons suggests impaired retrograde transport of autophagosomes and impaired degradation of damaged mitochondria as early as at P40. Our findings provide a clue as to why inducing autophagy alone, without compensatory rescue of LE transport and lysosomal deficits, failed to reduce mutant hSOD1 aggregates in the spinal MNs. Instead it augments MN degeneration and disease progression (Zhang et al., 2011), possibly due to enhanced autophagic stress and mitochondrial pathology. Our recent study revealed that the LE-loaded dynein-snapin complex drives the retrograde transport of axonal autophagosomes upon their fusion into amphisomes (Cheng et al., 2015). Efficient dynein-snapin coupling may help remove axonal autophagosomes engulfing aggregated proteins and dysfunctional organelles. Accumulation of vacuolated and dysfunctional mitochondria within distal axons early in the disease course can have catastrophic consequences by triggering axonal degeneration and denervation. This view is consistent with the notion that ALS is a dying-back type of neuropathy that initiates and progresses from distal to proximal portions of MNs (Fischer et al., 2004). Such early autophagic stress and mitochondrial pathology expedite progressive MN degeneration. Therefore, enhancing lysosomal function, rather than autophagy induction, is an alternative therapeutic strategy for ALS-linked clinical trials.

Impaired Retrograde Transport Underlying Autophagy-Lysosomal Deficits

Intracellular transport is fundamental for maintaining neuronal homeostasis and survival. In axons, dynein is a minus-end-directed motor that drives the retrograde transport of degradative organelles from axonal terminals to the soma where mature lysosomes are mainly localized, thus facilitating endolysosome membrane trafficking and lysosomal maturation (Ravikumar et al., 2005). Altered axonal transport was implicated in the ALS-associated pathogenesis (De Vos et al., 2007; Perlson et al., 2009; Williamson and Cleveland, 1999). In vivo analysis demonstrated axonal retrograde transport deficits in sciatic MNs, but not in sciatic DRG sensory neurons, of presymptomatic hSOD1^{G93A} mice (Bilsland et al., 2010). These deficits become even worse at the symptomatic stage. Consistently, mutations in dynein motors or genes that regulate dynein-mediated retrograde transport cause fALS-like pathology and MN degeneration in mice and human patients (Dion et al., 2009; Hafezparast et al., 2003). Defects in retrograde transport retain late endocytic organelles and immature AVs engulfing damaged mitochondria and protein aggregates within axons, rather than being delivered to the soma for degradation. This is confirmed by our TEM observations showing an aberrant accumulation of autophagy-mitophagy intermediates in ventral root axons, and by our immunohistostaining showing clustered LC3-labeled AVs, some of which colocalized with mitochondria, within axons of the crossed hSOD1^{G93A}/GFP-LC3 mice. Thus, our study provides clues that dynein-driven LE transport is essential for maturation and degradation of the autophagy-lysosome system in MNs.

Mutant hSOD1 Impairs Retrograde Transport by Interfering with the Snapin-Dynein Complex

Our findings prompt us to address mechanistic questions as to how mutant hSOD1 impairs LE transport and how snapin rescues this transport deficit. Mutant hSOD1 forms aggregates with the dynein complexes in the spinal MNs of asymptomatic hSOD1^{G93A} mice, and these aggregates interfere with axonal transport (Ligon et al., 2005; Sasaki et al., 2005). Three mutant forms of hSOD1 (G93A, G85R, and A4V), but not WT hSOD1^{WT}, interact with the DIC (Zhang et al., 2007). These mutant hSOD1-DIC complexes were readily found in fALS-linked mice at the presymptomatic stages and increased with disease progression (Ström et al., 2008), suggesting that dynein is a possible target of mutant hSOD1 toxicity. However, these studies raise a mechanistic question as to whether mutant hSOD1 aggregates interfere with the dynein-cargo attachment. It is particularly relevant because snapin acts as a dynein adaptor specific for LEs via binding the DIC (Cai et al., 2010). We propose that the hSOD1^{G93A}-DIC interaction interferes with snapin-DIC-mediated recruitment of dynein motors to LEs, thus reducing their retrograde transport in hSOD1^{G93A} MNs (Figure 5I).

We found reduced association of dynein DIC with Rab7-labeled late endocytic organelles in P40 hSOD1^{G93A} spinal cords compared to those from age-matched WT mice. Such reduced dynein tethering to LEs was not observed in age-matched hSOD1^{wt} transgenic mice, suggesting a phenotype specifically associated with hSOD1^{G93A} expression. Expressing snapin inhibits the hSOD1^{G93A}-DIC coupling, indicating competitive binding of snapin and hSOD1^{G93A} with the DIC. Thus, our study reveals a new mechanistic pathway through which mutant hSOD1 selectively impairs LE retrograde transport, which can be reversed by elevated snapin expression. We further showed that introducing *snapin* transgene into cultured adult MNs and an in vivo mouse model rescued autophagy-lysosomal deficits, facilitated removal of damaged mitochondria, and reduced MN death. Importantly, AAV9-snapin injection improved the motor coordination and prolonged the average lifespan of hSOD1^{G93A} mice for 12 days in the current study. This is comparable to those studies that, by directly inhibiting cytochrome *c*-induced MN apoptosis (Zhu et al., 2002) or by reducing the disease-modifier Epha4 signaling (Van Hoecke et al., 2012), both increased survival for about 11 days in the same mouse model. Therefore, enhancing dynein-mediated LE retrograde transport

rescues autophagy-lysosomal deficits caused by hSOD1^{G93A} and ameliorates the disease phenotype in this disease mouse model.

Because snapin plays multivalent roles in intracellular trafficking, we cannot exclude the possibility that it also improves MN viability through other trafficking pathways, such as synaptic vesicle trafficking and synchronized fusion (Pan et al., 2009) and retrograde transport of signaling endosomes (Zhou et al., 2012). Interestingly, expressing the snapin^{L99K} mutant defective in DIC binding failed to rescue autophagy-lysosomal deficits or reduce cell death in hSOD1^{G93A} MNs, further supporting that snapin/dynein-mediated transport plays a major role in restoring autophagy-lysosomal function and delaying MN degeneration.

In summary, our study reveals that lysosomal deficits and mitochondrial pathology in early asymptomatic hSOD1^{G93A} MNs are attributable to mutant hSOD1-induced impairment of endolysosomal trafficking. These early pathological changes impair the degradation of damaged mitochondria from distal axons of spinal MNs, thus causing them to be more vulnerable to dying-back degeneration. Elucidation of this early pathological mechanism is broadly relevant, because defective retrograde transport, lysosomal deficits, autophagic stress, and mitochondrial pathology are all associated with major neurodegenerative diseases, including ALS, Huntington's, Parkinson's, and Alzheimer's diseases (Nixon, 2013). Therefore, enhancing clearance of damaged mitochondria and mutant protein aggregates by regulating endolysosomal trafficking may be a potential therapeutic strategy for ALS and perhaps other neurodegenerative diseases.

EXPERIMENTAL PROCEDURES

Additional information can be found in the Supplemental Experimental Procedures.

Mouse Lines

B6.Cg-Tg (SOD1^{G93A})1Gur/J mice expressing high copy number of the G93A mutant form of human SOD1 and B6SJL-Tg(SOD1)2Gur/J mice expressing WT human SOD1 were purchased from The Jackson Laboratory. Animal care and use were carried out in accordance with NIH guidelines and approved by the NIH, NINDS/NIDCD Animal Care and Use Committee.

Adult MN Cultures

Mouse spinal cords were extruded from the decapitated neck and sectioned transversely at 500-μm thickness. After dissociation with 36 units/ml papain and 0.02% DNase I for 30 min at 30°C, the tissue suspension was centrifuged and the pellet was triturated three times with glass pipettes. After cell debris and tissue pieces were filtered through a 70-μm cell strainer, the MN suspension was enriched through OptiPrep gradient centrifugation and was re-suspended and plated on coverslips coated with 30 μg/ml poly-L-ornithine and 1 μg/ml laminin. MNs from paired WT and SOD1^{G93A} littermates at early asymptomatic ages (P40 or P65) were plated on coverslips at the density of 1,000 cells per 12-mm coverslip.

Assays for Mature Cathepsins B and D

To label active cathepsin D in mature lysosomes, live adult MNs or DRG neurons were incubated with 1 μM Bodipy FL-pepstatin A in culture medium for 1 hr at 37°C. The active form of cathepsin B was labeled by the cresyl violet fluorogenic substrate CV-(Arg-Arg)2 (Magic Red). Briefly, live neurons were incubated with staining solution (MR-RR2) at 1:1,300 dilution for 15 min at 37°C, then washed three times by HA medium for imaging. Reduced staining of Bodipy FL-pepstatin A or Magic Red in neurons reflects impaired lysosomal maturation.

Assay for Autophagic Maturation

Neurons were infected with lentivirus expressing mRFP-GFP-LC3. As soon as autophagy is induced, GFP, but not mRFP, undergoes rapid degradation in mature autolysosomes. Lysosomal defects result in both GFP and mRFP colocalized signals retained in immature autophagosomes. Colocalization between RFP-LC3 and GFP-LC3 signals was analyzed using ImageJ JACoP (NIH) with Mander's overlap coefficient. The signals were extracted from background by setting an appropriate threshold and by applying Gaussian blur to remove the background noise. Mander's overlap coefficient was calculated as the percentage of pixel intensity of GFP merged with RFP relative to the total RFP intensity, with 1 being full colocalization and 0 indicating no colocalization.

Statistical Analysis

Statistical analysis was carried out using Prism (GraphPad). Two groups were compared using F test or Mann-Whitney (sample size $n < 30$) or Student's t test (sample size $n \geq 30$). Data are expressed as mean ± SEM. Differences were considered significant with $p < 0.05$.

SUPPLEMENTAL INFORMATION

Supplemental Information includes Supplemental Experimental Procedures and seven figures and can be found with this article online at http://dx.doi.org/10.1016/j.neuron.2015.06.026.

AUTHOR CONTRIBUTIONS

Y.X. conducted experiments and data analysis in brain/spinal sections and in vivo studies. B.Z. conducted experiments and data analysis in adult cultured MNs. M.-Y.L. performed immuno-isolation and biochemical analysis. S.W. performed EM imaging. K.D.F. designed and prepared AAV9-snapin vectors for viral injection. Z.-H.S. is the senior author who designed the project. Y.X. and Z.-H.S. wrote the manuscript.

ACKNOWLEDGMENTS

We thank members of the Z.-H.S. lab for technical assistance and discussion; S. Cheng, R. Azzam, and V. Crocker at the NINDS Electron Microscopy Facility for assistance in TEM analysis; and D. Schoenberg for editing. The work was supported by the Intramural Research Program of NINDS, NIH ZIA NS003029, and ZIA NS002946 (Z.-H.S.).

Received: December 4, 2013
Revised: May 5, 2015
Accepted: June 16, 2015
Published: July 15, 2015

REFERENCES

Beal, M.F. (1996). Mitochondria, free radicals, and neurodegeneration. Curr. Opin. Neurobiol. *6*, 661–666.

Bilsland, L.G., Sahai, E., Kelly, G., Golding, M., Greensmith, L., and Schiavo, G. (2010). Deficits in axonal transport precede ALS symptoms in vivo. Proc. Natl. Acad. Sci. USA *107*, 20523–20528.

Boland, B., Kumar, A., Lee, S., Platt, F.M., Wegiel, J., Yu, W.H., and Nixon, R.A. (2008). Autophagy induction and autophagosome clearance in neurons: relationship to autophagic pathology in Alzheimer's disease. J. Neurosci. *28*, 6926–6937.

Cai, Q., Lu, L., Tian, J.-H., Zhu, Y.-B., Qiao, H., and Sheng, Z.-H. (2010). Snapin-regulated late endosomal transport is critical for efficient autophagy-lysosomal function in neurons. Neuron *68*, 73–86.

Castillo, K., Nassif, M., Valenzuela, V., Rojas, F., Matus, S., Mercado, G., Court, F.A., van Zundert, B., and Hetz, C. (2013). Trehalose delays the

progression of amyotrophic lateral sclerosis by enhancing autophagy in motoneurons. Autophagy *9*, 1308–1320.

Chen, H., and Chan, D.C. (2009). Mitochondrial dynamics–fusion, fission, movement, and mitophagy–in neurodegenerative diseases. Hum. Mol. Genet. *18* (R2), R169–R176.

Cheng, X.-T., Zhou, B., Lin, M.Y., Cai, Q., and Sheng, Z.-H. (2015). Axonal autophagosomes recruit dynein for retrograde transport through fusion with late endosomes. J. Cell Biol. *209*, 377–386.

Chiò, A., Borghero, G., Calvo, A., Capasso, M., Caponnetto, C., Corbo, M., Giannini, F., Logroscino, G., Mandrioli, J., Marcello, N., et al.; LITALS Study Group (2010). Lithium carbonate in amyotrophic lateral sclerosis: lack of efficacy in a dose-finding trial. Neurology *75*, 619–625.

Cleveland, D.W., and Rothstein, J.D. (2001). From Charcot to Lou Gehrig: deciphering selective motor neuron death in ALS. Nat. Rev. Neurosci. *2*, 806–819.

Cozzolino, M., Ferri, A., Valle, C., and Carrì, M.T. (2013). Mitochondria and ALS: implications from novel genes and pathways. Mol. Cell. Neurosci. *55*, 44–49.

De Vos, K.J., Chapman, A.L., Tennant, M.E., Manser, C., Tudor, E.L., Lau, K.-F., Brownlees, J., Ackerley, S., Shaw, P.J., McLoughlin, D.M., et al. (2007). Familial amyotrophic lateral sclerosis-linked SOD1 mutants perturb fast axonal transport to reduce axonal mitochondria content. Hum. Mol. Genet. *16*, 2720–2728.

Dion, P.A., Daoud, H., and Rouleau, G.A. (2009). Genetics of motor neuron disorders: new insights into pathogenic mechanisms. Nat. Rev. Genet. *10*, 769–782.

Fischer, L.R., Culver, D.G., Tennant, P., Davis, A.A., Wang, M., Castellano-Sanchez, A., Khan, J., Polak, M.A., and Glass, J.D. (2004). Amyotrophic lateral sclerosis is a distal axonopathy: evidence in mice and man. Exp. Neurol. *185*, 232–240.

Fornai, F., Longone, P., Cafaro, L., Kastsiuchenka, O., Ferrucci, M., Manca, M.L., Lazzeri, G., Spalloni, A., Bellio, N., Lenzi, P., et al. (2008). Lithium delays progression of amyotrophic lateral sclerosis. Proc. Natl. Acad. Sci. USA *105*, 2052–2057.

Foust, K.D., Wang, X., McGovern, V.L., Braun, L., Bevan, A.K., Haidet, A.M., Le, T.T., Morales, P.R., Rich, M.M., Burghes, A.H.M., and Kaspar, B.K. (2010). Rescue of the spinal muscular atrophy phenotype in a mouse model by early postnatal delivery of SMN. Nat. Biotechnol. *28*, 271–274.

Gal, J., Ström, A.-L., Kilty, R., Zhang, F., and Zhu, H. (2007). p62 accumulates and enhances aggregate formation in model systems of familial amyotrophic lateral sclerosis. J. Biol. Chem. *282*, 11068–11077.

Gill, A., Kidd, J., Vieira, F., Thompson, K., and Perrin, S. (2009). No benefit from chronic lithium dosing in a sibling-matched, gender balanced, investigator-blinded trial using a standard mouse model of familial ALS. PLoS ONE *4*, e6489.

Gurney, M.E., Pu, H., Chiu, A.Y., Dal Canto, M.C., Polchow, C.Y., Alexander, D.D., Caliendo, J., Hentati, A., Kwon, Y.W., Deng, H.X., et al. (1994). Motor neuron degeneration in mice that express a human Cu,Zn superoxide dismutase mutation. Science *264*, 1772–1775.

Hafezparast, M., Klocke, R., Ruhrberg, C., Marquardt, A., Ahmad-Annuar, A., Bowen, S., Lalli, G., Witherden, A.S., Hummerich, H., Nicholson, S., et al. (2003). Mutations in dynein link motor neuron degeneration to defects in retrograde transport. Science *300*, 808–812.

Hariri, M., Millane, G., Guimond, M.P., Guay, G., Dennis, J.W., and Nabi, I.R. (2000). Biogenesis of multilamellar bodies via autophagy. Mol. Biol. Cell *11*, 255–268.

Harris, H., and Rubinsztein, D.C. (2012). Control of autophagy as a therapy for neurodegenerative disease. Nat. Rev. Neurol. *8*, 108–117.

Ilieva, H., Polymenidou, M., and Cleveland, D.W. (2009). Non-cell autonomous toxicity in neurodegenerative disorders: ALS and beyond. J. Cell Biol. *187*, 761–772.

Kang, J.-S., Tian, J.-H., Pan, P.-Y., Zald, P., Li, C., Deng, C., and Sheng, Z.-H. (2008). Docking of axonal mitochondria by syntaphilin controls their mobility and affects short-term facilitation. Cell *132*, 137–148.

Kiselyov, K., Jennigs, J.J., Jr., Rbaibi, Y., and Chu, C.T. (2007). Autophagy, mitochondria and cell death in lysosomal storage diseases. Autophagy *3*, 259–262.

Lambrechts, D., Storkebaum, E., Morimoto, M., Del-Favero, J., Desmet, F., Marklund, S.L., Wyns, S., Thijs, V., Andersson, J., van Marion, I., et al. (2003). VEGF is a modifier of amyotrophic lateral sclerosis in mice and humans and protects motoneurons against ischemic death. Nat. Genet. *34*, 383–394.

Lee, S., Sato, Y., and Nixon, R.A. (2011). Lysosomal proteolysis inhibition selectively disrupts axonal transport of degradative organelles and causes an Alzheimer's-like axonal dystrophy. J. Neurosci. *31*, 7817–7830.

Li, L., Zhang, X., and Le, W. (2008). Altered macroautophagy in the spinal cord of SOD1 mutant mice. Autophagy *4*, 290–293.

Ligon, L.A., LaMonte, B.H., Wallace, K.E., Weber, N., Kalb, R.G., and Holzbaur, E.L.F. (2005). Mutant superoxide dismutase disrupts cytoplasmic dynein in motor neurons. Neuroreport *16*, 533–536.

Maday, S., Wallace, K.E., and Holzbaur, E.L.F. (2012). Autophagosomes initiate distally and mature during transport toward the cell soma in primary neurons. J. Cell Biol. *196*, 407–417.

Magrané, J., and Manfredi, G. (2009). Mitochondrial function, morphology, and axonal transport in amyotrophic lateral sclerosis. Antioxid. Redox Signal. *11*, 1615–1626.

Marinkovic, P., Reuter, M.S., Brill, M.S., Godinho, L., Kerschensteiner, M., and Misgeld, T. (2012). Axonal transport deficits and degeneration can evolve independently in mouse models of amyotrophic lateral sclerosis. Proc. Natl. Acad. Sci. USA *109*, 4296–4301.

Mizushima, N., Yamamoto, A., Matsui, M., Yoshimori, T., and Ohsumi, Y. (2004). In vivo analysis of autophagy in response to nutrient starvation using transgenic mice expressing a fluorescent autophagosome marker. Mol. Biol. Cell *15*, 1101–1111.

Morimoto, N., Nagai, M., Ohta, Y., Miyazaki, K., Kurata, T., Morimoto, M., Murakami, T., Takehisa, Y., Ikeda, Y., Kamiya, T., and Abe, K. (2007). Increased autophagy in transgenic mice with a G93A mutant SOD1 gene. Brain Res. *1167*, 112–117.

Mórotz, G.M., De Vos, K.J., Vagnoni, A., Ackerley, S., Shaw, C.E., and Miller, C.C.J. (2012). Amyotrophic lateral sclerosis-associated mutant VAPBP56S perturbs calcium homeostasis to disrupt axonal transport of mitochondria. Hum. Mol. Genet. *21*, 1979–1988.

Nixon, R.A. (2013). The role of autophagy in neurodegenerative disease. Nat. Med. *19*, 983–997.

Osellame, L.D., and Duchen, M.R. (2014). Quality control gone wrong: mitochondria, lysosomal storage disorders and neurodegeneration. Br. J. Pharmacol. *171*, 1958–1972.

Pan, P.-Y., Tian, J.-H., and Sheng, Z.-H. (2009). Snapin facilitates the synchronization of synaptic vesicle fusion. Neuron *61*, 412–424.

Perlson, E., Jeong, G.B., Ross, J.L., Dixit, R., Wallace, K.E., Kalb, R.G., and Holzbaur, E.L.F. (2009). A switch in retrograde signaling from survival to stress in rapid-onset neurodegeneration. J. Neurosci. *29*, 9903–9917.

Pizzasegola, C., Caron, I., Daleno, C., Ronchi, A., Minoia, C., Carrì, M.T., and Bendotti, C. (2009). Treatment with lithium carbonate does not improve disease progression in two different strains of SOD1 mutant mice. Amyotroph. Lateral Scler. *10*, 221–228.

Ravikumar, B., Acevedo-Arozena, A., Imarisio, S., Berger, Z., Vacher, C., O'Kane, C.J., Brown, S.D.M., and Rubinsztein, D.C. (2005). Dynein mutations impair autophagic clearance of aggregate-prone proteins. Nat. Genet. *37*, 771–776.

Rosen, D.R., Siddique, T., Patterson, D., Figlewicz, D.A., Sapp, P., Hentati, A., Donaldson, D., Goto, J., O'Regan, J.P., Deng, H.X., et al. (1993). Mutations in Cu/Zn superoxide dismutase gene are associated with familial amyotrophic lateral sclerosis. Nature *362*, 59–62.

Sarkar, S., Floto, R.A., Berger, Z., Imarisio, S., Cordenier, A., Pasco, M., Cook, L.J., and Rubinsztein, D.C. (2005). Lithium induces autophagy by inhibiting inositol monophosphatase. J. Cell Biol. *170*, 1101–1111.

Sasaki, S., Warita, H., Murakami, T., Shibata, N., Komori, T., Abe, K., Kobayashi, M., and Iwata, M. (2005). Ultrastructural study of aggregates in the spinal cord of transgenic mice with a G93A mutant SOD1 gene. Acta Neuropathol. *109*, 247–255.

Settembre, C., Fraldi, A., Jahreiss, L., Spampanato, C., Venturi, C., Medina, D., de Pablo, R., Tacchetti, C., Rubinsztein, D.C., and Ballabio, A. (2008). A block of autophagy in lysosomal storage disorders. Hum. Mol. Genet. *17*, 119–129.

Shan, X., Chiang, P.-M., Price, D.L., and Wong, P.C. (2010). Altered distributions of Gemini of coiled bodies and mitochondria in motor neurons of TDP-43 transgenic mice. Proc. Natl. Acad. Sci. USA *107*, 16325–16330.

Sheng, Z.-H., and Cai, Q. (2012). Mitochondrial transport in neurons: impact on synaptic homeostasis and neurodegeneration. Nat. Rev. Neurosci. *13*, 77–93.

Ström, A.-L., Shi, P., Zhang, F., Gal, J., Kilty, R., Hayward, L.J., and Zhu, H. (2008). Interaction of amyotrophic lateral sclerosis (ALS)-related mutant copper-zinc superoxide dismutase with the dynein-dynactin complex contributes to inclusion formation. J. Biol. Chem. *283*, 22795–22805.

Van Hoecke, A., Schoonaert, L., Lemmens, R., Timmers, M., Staats, K.A., Laird, A.S., Peeters, E., Philips, T., Goris, A., Dubois, B., et al. (2012). EPHA4 is a disease modifier of amyotrophic lateral sclerosis in animal models and in humans. Nat. Med. *18*, 1418–1422.

Williamson, T.L., and Cleveland, D.W. (1999). Slowing of axonal transport is a very early event in the toxicity of ALS-linked SOD1 mutants to motor neurons. Nat. Neurosci. *2*, 50–56.

Wootz, H., Weber, E., Korhonen, L., and Lindholm, D. (2006). Altered distribution and levels of cathepsinD and cystatins in amyotrophic lateral sclerosis transgenic mice: possible roles in motor neuron survival. Neuroscience *143*, 419–430.

Zhang, F., Ström, A.L., Fukada, K., Lee, S., Hayward, L.J., and Zhu, H. (2007). Interaction between familial amyotrophic lateral sclerosis (ALS)-linked SOD1 mutants and the dynein complex. J. Biol. Chem. *282*, 16691–16699.

Zhang, X., Li, L., Chen, S., Yang, D., Wang, Y., Zhang, X., Wang, Z., and Le, W. (2011). Rapamycin treatment augments motor neuron degeneration in SOD1(G93A) mouse model of amyotrophic lateral sclerosis. Autophagy *7*, 412–425.

Zhou, B., Cai, Q., Xie, Y., and Sheng, Z.-H. (2012). Snapin recruits dynein to BDNF-TrkB signaling endosomes for retrograde axonal transport and is essential for dendrite growth of cortical neurons. Cell Rep. *2*, 42–51.

Zhu, Y.B., and Sheng, Z.H. (2011). Increased axonal mitochondrial mobility does not slow amyotrophic lateral sclerosis (ALS)-like disease in mutant SOD1 mice. J. Biol. Chem. *286*, 23432–23440.

Zhu, S., Stavrovskaya, I.G., Drozda, M., Kim, B.Y.S., Ona, V., Li, M., Sarang, S., Liu, A.S., Hartley, D.M., Wu, D.C., et al. (2002). Minocycline inhibits cytochrome c release and delays progression of amyotrophic lateral sclerosis in mice. Nature *417*, 74–78.